

Model Matching Control for an Active-Passive Variable Stiffness Actuator

Po-Jen Cheng

*Department of Mechanical Engineering
National Taiwan University
Taipei, 10617, Taiwan*

u9014028@gmail.com

H.P. Huang

*Department of Mechanical Engineering
National Taiwan University
Taipei, 10617, Taiwan*

hanpang@ntu.edu.tw

Abstract

In order to increase the safety performance between human and the robot, the variable stiffness mechanism is commonly adopted due to its flexibility in various tasks. However, it makes the actuator more complex and increases the weight of the system. To deal with this problem, the active-passive variable stiffness elastic actuator (APVSEA) [1] and the variable stiffness control that uses a model matching control (MMC) with bond graph are proposed in this article. The APVSEA is modeled as a non-back drivable bond graph model. Combining the MMC with the non-back drivable bond graph model, the overall system can achieve active stiffness control. The simulations and the experiments show good control performance. They prove that the proposed method can achieve active stiffness control well. In the future, the proposed method can also be applied to the robot arm and exoskeletons for balancing safety and the control performance.

Keywords: Serial Elastic Actuator, Bond Graph, Model Matching Control.

1. INTRODUCTION

Robots will not only exist in factories but will also service in our life in the near future. They will help humans and interact with people directly, for example, security in companies, home care, restaurant service, and rehabilitation in patients' homes. Traditionally, the properties of industrial robots have been heavy, fast, and powerful. Those industrial robots have no capacity for safe interaction with humans. Therefore, a robot that achieves precision and high-speed performance is becoming an important issue. In order to interact with humans, researchers in the robotics field have been focused on human-robot interaction (HRI) in the past decade. To guarantee safety during the human-robot interaction, several approaches dealing with this problem have been developed.

Recently, researchers tried to develop intrinsically safe robot actuation. One approach is to use a serial elastic actuator (SEA) between human and the robot. The effect of SEA is to absorb impact force during HRI [2-4]. SEA uses elastic elements between transmission mechanisms and loads serially, and [5-7] have presented both linear and rotary SEA designs.

The main problem in SEA is that the stiffness is constant. The constant stiffness limits the dynamic range of force control and makes the SEA unusable in many daily activities in human life. Therefore, the variable stiffness system is important for dealing with variable tasks. To achieve the variable stiffness property, some researchers purposed the concept of a variable stiffness elastic actuator (VSEA) for robot manipulation and interaction between human and the robot [8-9]. In [10-13], the safe link mechanism (SLM) and safe joint mechanism (SJM) combined with the slider structure, transmission shafts, and non-linear springs were proposed to achieve

collision safety. The actuator performs nonlinear characteristics by using the four-bar linkage and slider mechanism in combination with springs. The variable stiffness actuator adopts a variable stiffness transmission to change mechanism stiffness. Migliore purposed an approach that allows to change the mechanism's stiffness using two non-linear springs working in an antagonistic configuration [14]. In order to control the position and stiffness of the system, some researchers used two actuators to change the effective length of the spring or link position [15-16].

The common problem in realizing the mechanism with VSEA is that the system will become heavy with huge volume. In [17], the actuator of the robot is a pneumatic artificial muscle which is flexible and has a light weight. However, the variable stiffness property is limited.

To develop an effective active variable stiffness system, we adopt bond graph and model matching controller (MMC) to model the SEA system and to achieve the variable stiffness control [19-22]. Bond graph is an excellent model language that can describe multi-domain physical dynamic systems. It also has extension ability and can accomplish mechatronics design or integrate multi-domain models easily. In reference [18], Hernani modeled Hill's muscle model using bond graph and extended the unit muscle model to the human gait musculoskeletal system.

There have been many SEA studies in the past. However, few papers discuss SEA modeling using bond graph. In this paper, the active-passive variable stiffness elastic actuator (APVSEA) [1], developed by our laboratory, will be introduced first. We model the non-back drivable APVSEA based on bond graph. It can be served as a module for future development.

The aims of MMC are to generate a reference model and make the plant's output approximate the reference model's response. Nevertheless, there are few literatures to describe the design flow and step of MMC using bond graph and apply to the SEA system. In this paper, the APVSEA system is the first modeled using bond graph and the design of the MMC controller is followed.

The paper is organized as follows. In Section II, the principle and properties of the active-passive variable stiffness actuator (APVSEA) are introduced [1] and modeled using bond graph. The MMC controller design is applied to the APVSEA through the model of the APVSEA in Section III. In addition, the system's solvability, the inverse system, and the disturbance decouple problem (DDP) will also be addressed. In Section IV, the analysis and simulation of the MMC will be conducted. The MMC controller will be realized in the APVSEA, and experiment results will be shown in Section V. The last section draws our conclusions.

2. APVSEA OPERATION PRINCIPLE AND MODEL

It is necessary to deeply understand APVSEA system before designing bond graph. In this section, the operational principle of the APVSEA will be described and the bond graph representation of the APVSEA will be conducted.

2.1 APVSEA Operation Principle [1]

The APVSEA is a human-robot interaction mechanism with intrinsic safety properties. It was developed by our laboratory. The APVSEA system, shown in figure 1, has two different parts: one is SEA; the other can change the system's stiffness. APVSEA can actively or passively change the mechanism's stiffness to satisfy the human-robot interaction requirement. APVSEA consists of two DC motors, one ball screw, one driving screw, and four springs. The potentiometer above the spring is used to measure spring displacement and three encoders can measure motor 01, motor 02, and the output link angle. The main goal of motor 02 is to change the stiffness of the APVSEA. However, this paper is focused on the SEA system and varies system stiffness using the MMC controller. Therefore, this paper will not discuss the functional part of motor 02 that changes the APVSEA stiffness.

Figure 1 shows how APVSEA drivers' output is linked to motor 01. First, motor 01 rotates the ball screw through time belt 01. Second, the ball screw moves the moving plant forward or backward. Finally, the moving plant pulls timing belt 02 to rotate output link, as shown in figure 2.

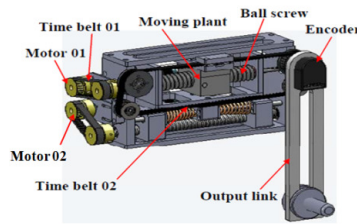


FIGURE 1: APVSEA 3D diagram

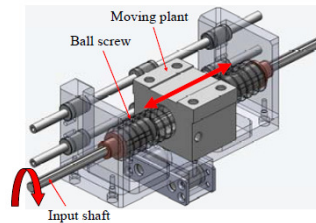


FIGURE 2: Moving Plant is Moved by Motor 01.

If there are some external forces on the output link, the external forces will drive the moving plant using timing belt 02. However, because the moving plant cannot drive the ball screw back, the external forces generate axial force and make the ball screw and the moving plant slip on the input shaft. As the translation of the moving plant occurs, the springs in the APVSEA absorb those external forces through the connector, as shown in Figs. 3 and 4. This is the SEA property which means the APVSEA can absorb an external force so that the human interacts with the robot safely. The detailed specification of the APVSEA is listed in Table I.

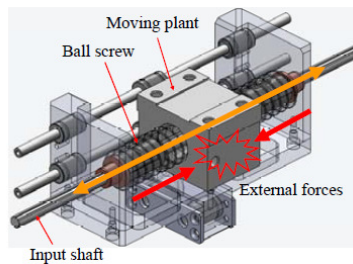


FIGURE 3: External Force Generates Axial Slipping Motion.

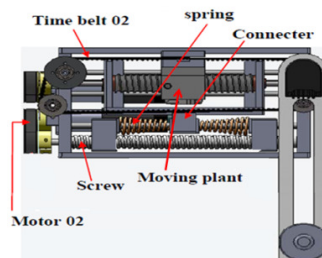


FIGURE 4: The Spring Absorb Forces from External Environment.

PARAMETERS	VALUES
Mass (includes two motors)	2.2kg
Length*Width*Height	200*100*116 mm
Number of DC-motors	2
Max. Output Torque	29Nm
Max. Output Speed	24rpm
Spring Stiffness	152N/mm
Max. Output Link Deflection	$\pm 90^\circ$

TABLE 1: The Specification of APVSEA.

2.2 Model APVSEA by Bond Graph

From the discussion above, the user applies external force to the output link, and motor 01 simultaneously drives the output link. Because the APVSEA is a non-back drivable system, the external force applied by the user cannot affect motor 01.

In order to simplify the APVSEA system, we can treat the system as the user pushes a mass-damper-spring system in a car. Because the user's force is internal, it cannot move the car forward, as shown in figure 5. In other words, the car can change the human's absolute position, but human force cannot move the car. The simplified APVSEA model is shown in figure 6. \tilde{u} is the car velocity (i.e., \tilde{u} is the angular velocity from motor 01 .)

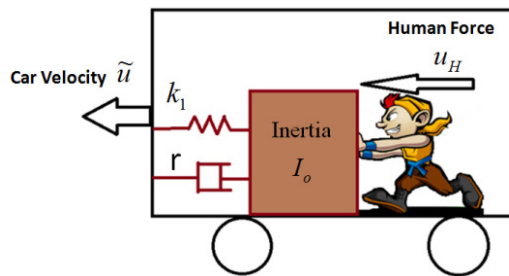


FIGURE 5: The APVSEA system can be described as human is pushing mass-damper-spring system in a car.

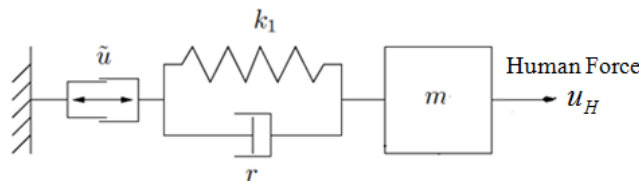


FIGURE 6: The Simplified APVSEA Model.

Based on the simplified APVSEA model, the system's model is constructed using bond graph, as shown in figure 7. \dot{x}_1 and \dot{x}_2 represent the force applied to output link and spring velocity, respectively. SS is a source-sensor element. Se and Sf define the effort source and flow source, respectively. The parameters m , k_1 and r are defined as mass, spring stiffness and damping ratio, respectively.

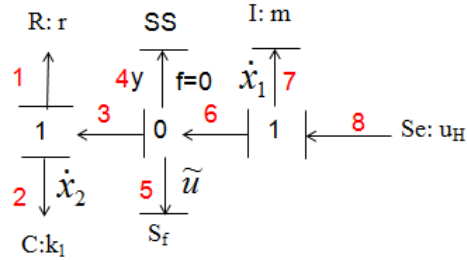


FIGURE 7: The APVSEA Bond Graph Diagram.

According to the Port-Hamiltonian dynamic equation [19], the following dynamic equation (1) is derived from the bond graph:

$$\begin{bmatrix} \dot{x}_1 \\ \dot{x}_2 \end{bmatrix} = \begin{bmatrix} -r & -1 \\ 1 & 0 \end{bmatrix} \nabla H(x) - \begin{bmatrix} -1 & -r \\ 0 & 1 \end{bmatrix} u \tag{1}$$

$$y = [r \quad 1] \nabla H(x) + [0 \quad r] u$$

where $u = (u_H, \tilde{u})^T$ and the Hamiltonian $H(x): x \rightarrow \mathfrak{R}$ is defined as $H(x) = (x_1^2/m + k_1 x_2^2)/2$, which is the energy function. The $\nabla H(x)$ is a column gradient vector.

Figure 7 is the bond graph model of the non-back drivable APVSEA system, where the terminal of \tilde{u} is the motor input, and u_H is the operator input external force, respectively. In the case of the APVSEA, \tilde{u} converts its power through the timing belt and ball-screw into a velocity that operates on a system spring. The developer can add the motor, electric drive, electric power, etc., behind \tilde{u} . We can also regard u_H as a human input force that can be extended to Hill’s muscle model. Therefore, the researcher can design a robot arm or exoskeleton system basing on the modular APVSEA model, as shown in figure 7. The I, C, R mean inertia, spring and damper in mechanical domain in bond graph, respectively. The junction elements are denoted as 1 and 0 (black number). The bond numbers are defined as red words in Figure 7. The total forces apply to output link is denoted as \dot{x}_1 and velocity of spring is denoted as \dot{x}_2 . Each arrow is used to indicate positive effort or flow direction.

3. MODEL MATCHING CONTROL (MMC)

The advantage of MMC is that the designer can specify the reference model’s response clearly. Bond graph offers an excellent model language. It can be used to design a reference model visually.

The MMC can be viewed as that there is a disturbance in the extended model system input \bar{u} . Therefore, the MMC seems to be a disturbance decouple problem (DDP). This means that the plant input $u(t)$ can decouple the model input $\bar{u}(t)$ and extend the system E to the output y_e . Figure 8 shows the flow chart of the MMC controller design.

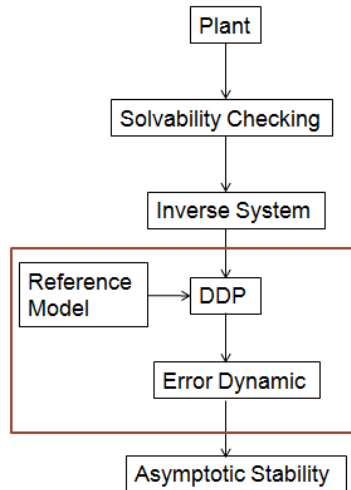


FIGURE 8: MMC Controller Design Flow Chart.

In this paper, the MMC controller is designed using bond graph. The first step is to construct a plant model using bond graph. The second step is to check the solvability of this plant. If the plant is solvable, the inverse system using a bi-causal bond graph can be obtained. If the system does not have an inverse system, we cannot find the MMC controller. Using the inverse system, we can solve DDP and derive an error dynamic equation. A new control input μ_i will force the error dynamic equation to equal zero.

According to the first-order differential function of the energy, we can confirm if this error system is an essential asymptotically stable system. Finally, we can determine if the asymptotic conditions satisfy the asymptotic stability by defining a new energy function $H_s(e)$ and control input in the shaped Hamiltonian.

3.1 Solvability Checking

In order to determine the system’s solvability, Wlasowski, and Lorenz proposed an approach that can check solvability using bond graph [23]. In this paper, we adopt this approach and derive the following matrix from figure 7 as

$$\begin{bmatrix} f_1 \\ f_2 \\ f_3 \end{bmatrix} = \begin{bmatrix} -1 & 1 \\ -1 & 1 \\ 0 & -1 \end{bmatrix} \begin{bmatrix} f_5 \\ f_7 \end{bmatrix} \equiv \widehat{F}f_{EJ} \tag{2}$$

$$\begin{bmatrix} e_4 \\ e_7 \end{bmatrix} = \begin{bmatrix} -1 & -1 & 0 \\ -1 & -1 & 1 \end{bmatrix} \begin{bmatrix} e_1 \\ e_2 \\ e_3 \end{bmatrix} \equiv \widehat{E}e_{EJ} \tag{3}$$

where f_i (e_i) means flow (effort) of the i -th bond from figure 7. The notation E means all bond graph environment elements (I, C, R) except for 0, 1, TF, and GY elements. J is the system’s 0-junction or 1-junction. Because there is no modulated bond graph element, we can convert equations (2) and (3) into the structure equation [23] as:

$$\begin{cases} f_{JE} = \hat{F}f_{EJ} \\ e_{JE} = \hat{E}e_{EJ} \end{cases} \quad (4)$$

where $e_{EJ}(f_{EJ})$ means the effort (flow) transmit direction from the environment to junction node. Similarly, the effort (flow) transmit direction from junction to environment node is represented as $e_{JE}(f_{JE})$. Because the structure equation (4) has no singular matrix, i.e., \hat{F} and \hat{E} have an inverse matrix, we can conclude the APVSEA is a solvable system and there exists an inverse system.

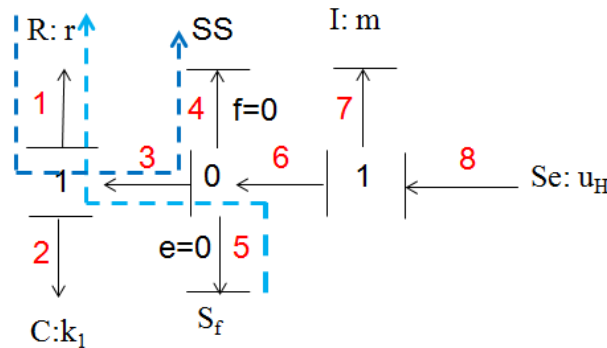


FIGURE 9: APVSEA's Power Line.

3.2 Inverse System

Since the APVSEA is solvable, there exists an inverse system. We can generate input-output power lines, as shown in figure 9, where the light blue dotted line is the flow direction and the deep blue one is the effort direction. Based on the power line, the inverse system of the APVSEA can be obtained using bi-causal bond graph, as shown in figure 10.

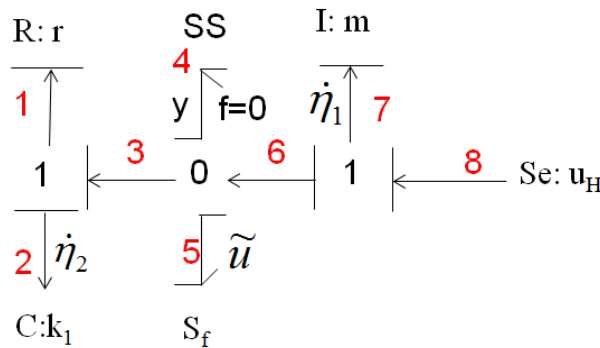


FIGURE 10: The Inverse System of APVSEA.

3.3 Reference Model

The reference model for the MMC is shown in figure 11. The bond graph of the reference model is given in figure 12. The MMC design will make the APVSEA match to the reference model. Here, the reference model not only preserves the APVSEA system, but also adds an extra spring k_d , which can vary the original system's stiffness. Form figure 12, we can derive the system dynamic equations as follows

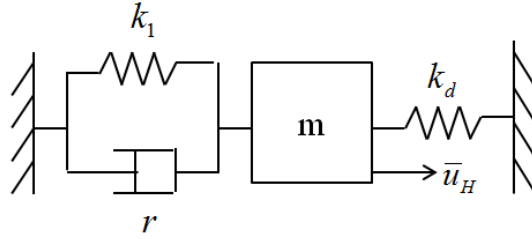


FIGURE 11: Reference Model Definition.

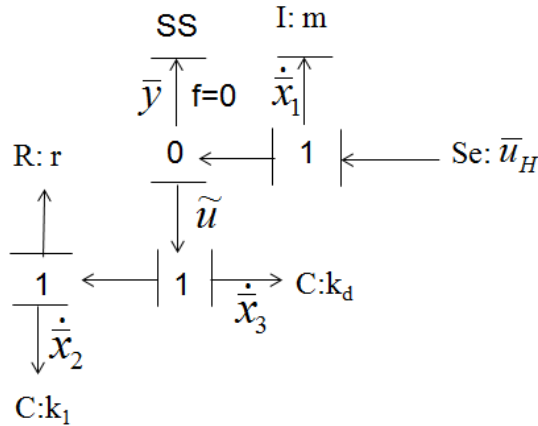


FIGURE 12 Reference Model Bond Graph.

$$\begin{bmatrix} \dot{\bar{x}}_1 \\ \dot{\bar{x}}_2 \\ \dot{\bar{x}}_3 \end{bmatrix} = \begin{bmatrix} -r & -1 & -1 \\ 1 & 0 & 0 \\ 1 & 0 & 0 \end{bmatrix} \nabla \bar{H}(\bar{x}) + \begin{bmatrix} 1 \\ 0 \\ 0 \end{bmatrix} \bar{u}_H \quad (5)$$

$$\bar{y} = [r \quad 1 \quad 1] \nabla \bar{H}(\bar{x})$$

where \bar{u}_H is an external force applied to the reference model. $\dot{\bar{x}}_1$ and $\dot{\bar{x}}_2$ represent the force which apply to output link and spring velocity, respectively. The Hamiltonian $\bar{H}(\bar{x}): \bar{x} \rightarrow \mathfrak{R}$ is defined as $\bar{H}(\bar{x}) = (\bar{x}_1^2/m + k_1\bar{x}_2^2 + k_d\bar{x}_3^2)/2$, which is the reference model's energy function. The $\nabla \bar{H}(\bar{x})$ is a column gradient vector.

3.4 Disturbance Decouple Problem (DDP)

We can derive an inverse system relation equation from figure 10 directly as

$$\begin{aligned} \tilde{u} &= f_6 - f_3 = \frac{1}{m} \int \dot{\eta}_1 dt - \dot{\eta}_2 \\ &= \frac{1}{m} \left(\int (u_H - y) dt \right) - \frac{1}{r} (y - k_1 \eta_2) \end{aligned} \quad (6)$$

where η_1 and η_2 are storage elements dynamics in the inverse system. In order to solve DDP, the main concept of MMC is to match the dynamic parameters of the inverse system and the model, i.e., set $y = \bar{y}, u_H = \bar{u}_H$, where \bar{y} can be derived by substituting equation (5) to equation (6). \bar{u}_H is seen as a disturbance as

$$\tilde{u} = \frac{1}{m} \left(\int (\bar{u}_H - \bar{y}) dt \right) - \frac{1}{r} (\bar{y} - k_1 \eta_2) + \mu \quad (7)$$

where μ is a new control parameter and $\bar{y} = r\bar{x}_1/m + k_1\bar{x}_2 + k_d\bar{x}_3 = \bar{u}_H - \dot{\bar{x}}_1$. Equation (7) is rewritten as

$$\begin{aligned} \tilde{u} &= \frac{1}{m} \left(\int \dot{\bar{x}}_1 dt \right) - \frac{1}{r} (\bar{y} - k_1 \eta_2) + \mu \\ &= \frac{1}{m} \bar{x}_1 - \frac{1}{r} \left(\frac{r}{m} \bar{x}_1 + k_1 \bar{x}_2 + k_d \bar{x}_3 - k_1 \eta_2 \right) + \mu \end{aligned} \quad (8)$$

By setting $\bar{x}_2 = \eta_2$, equation (8) can be rewritten as

$$\tilde{u} = -\frac{1}{r} k_d \bar{x}_3 + \mu \quad (9)$$

There is a new control parameter μ in equation (9), which can make the plant asymptotically stable.

3.5 Error Dynamic

In order to generate the error dynamic equation, let $\varepsilon_1 = x_1 - \bar{x}_1$ and $\varepsilon_2 = x_2 - \bar{x}_2 = x_2 - \eta_2$.

$$\begin{aligned} \dot{\varepsilon}_1 &= \dot{x}_1 - \dot{\bar{x}}_1 \\ &= \left[\left(-\frac{r}{m} x_1 - k_1 x_2 \right) + u_H + r\tilde{u} \right] - (u_H - \bar{y}) \end{aligned} \quad (10)$$

where $\tilde{u} = -k_d \bar{x}_3 / r + \mu$. We rewrite equation (10) as

$$\begin{aligned} \dot{\varepsilon}_1 &= -\frac{r}{m} x_1 - k_1 x_2 + r\tilde{u} + \frac{r}{m} \bar{x}_1 + k_1 \bar{x}_2 + k_d \bar{x}_3 \\ &= -\frac{r}{m} (x_1 - \bar{x}_1) - k_1 (x_2 - \bar{x}_2) + k_d \bar{x}_3 + r \left(-\frac{1}{r} k_d \bar{x}_3 + \mu \right) \\ &= -\frac{r}{m} \varepsilon_1 - k_1 \varepsilon_2 + r\mu \end{aligned} \quad (11)$$

Similarly,

$$\begin{aligned} \dot{\varepsilon}_2 &= \dot{x}_2 - \dot{\eta}_2 = \frac{1}{m} x_1 - \tilde{u} - \frac{1}{r} (\bar{y} - k_1 \eta_2) \\ &= \frac{1}{m} x_1 + \frac{1}{r} k_d \bar{x}_3 - \mu - \frac{1}{r} \left(\frac{r}{m} \bar{x}_1 + k_1 \bar{x}_2 + k_d \bar{x}_3 - k_1 \eta_2 \right) \\ &= \frac{1}{m} \varepsilon_1 - \mu \end{aligned} \quad (12)$$

By combining equations (11) and (12), we can obtain the MMC error dynamic equation as

$$\begin{bmatrix} \dot{\varepsilon}_1 \\ \dot{\varepsilon}_2 \end{bmatrix} = \begin{bmatrix} -r & -1 \\ 1 & 0 \end{bmatrix} \nabla H(\varepsilon) + \begin{bmatrix} r \\ -1 \end{bmatrix} \mu \quad (13)$$

where $H(\varepsilon) = (\varepsilon_1^2/m + k_1\varepsilon_2^2)/2$ is the error energy function. The $\nabla H(\varepsilon)$ is a column gradient vector.

3.6 Asymptotic Stability

By setting the new control input $\mu = 0$ in equation (13), the differential equation is given as

$$\begin{aligned} \frac{d}{dt} H(\varepsilon) &= \varepsilon_1 \dot{\varepsilon}_1 / m + k_1 \varepsilon_2 \dot{\varepsilon}_2 \\ &= \varepsilon_1 (-r\varepsilon_1 / m - k_1\varepsilon_2) / m + k_1 \varepsilon_2 (\varepsilon_1 / m) \\ &= -r\varepsilon_1^2 / m \end{aligned} \quad (14)$$

Through observing equation (14), we know the MMC control system is asymptotically stable. However, the goal of adding a new controller μ is to force the system output $y(t)$ to close the model output $\bar{y}(t)$. Define a new energy function $H_s(\varepsilon)$ using the shaped Hamiltonian approach as

$$\begin{aligned} H_s(\varepsilon) &= H(\varepsilon) + c_1 \varepsilon_2^2 / 2 \\ &= \left[(\varepsilon_1^2 / m + k_1 \varepsilon_2^2) / 2 \right] + c_1 \varepsilon_2^2 / 2 \end{aligned} \quad (15)$$

where parameter c_1 is a constant.

In order to prove the stability, the energy function $H_s(\varepsilon)$ has to satisfy the following Lyapunov criteria.

Criterion 1: The energy function $H_s(\varepsilon)$ equals to zero at $\varepsilon = 0$.

$$H_s(0) = 0 \quad (16)$$

Criterion 2: According to equation (15), the energy function satisfies $H_s(\varepsilon) > 0$ for every input because the parameters m and k_1 are positive. So, satisfying the fulfillment of this criterion depends on parameter c_1 . The following criterion 3 is used for decision.

Criterion 3: The time derivative of $H_s(\varepsilon)$ is negative, i.e., $\frac{d}{dt} H_s(\varepsilon) < 0$.

$$\begin{aligned} \frac{d}{dt} H_s(\varepsilon) &= \frac{1}{m} \varepsilon_1 \dot{\varepsilon}_1 + k_1 \varepsilon_2 \dot{\varepsilon}_2 + c_1 \varepsilon_2 \dot{\varepsilon}_2 \\ &= \frac{1}{m} \varepsilon_1 \left[-\frac{r}{m} \varepsilon_1 - k_1 \varepsilon_2 + r\mu \right] + k_1 \varepsilon_2 \left(\frac{1}{m} \varepsilon_1 - \mu \right) + c_1 \varepsilon_2 \left(\frac{1}{m} \varepsilon_1 - \mu \right) \\ &= -\frac{r}{m^2} \varepsilon_1^2 + \frac{1}{m} \varepsilon_1 (r\mu + c_1 \varepsilon_2) - \varepsilon_2 \mu (k_1 + c_1) \end{aligned} \quad (17)$$

It is clear that when the goal of the MMC controller is achieved, the system is asymptotically stable. The stability condition requires $k_1 + c_1 = 0$, and $r\mu + c_1\varepsilon_2 = 0$. Therefore, $c_1 = -k_1$ and $\mu = k_1(x_2 - \bar{x}_2)/r$ is subject to equation (13). Based on those conditions, the system stability can be checked by the following equations

$$\begin{aligned} \dot{\varepsilon}_1 &= -\frac{r}{m}\varepsilon_1 - k_1\varepsilon_2 + r\mu \\ &= -\frac{r}{m}\varepsilon_1 \end{aligned} \tag{18}$$

$$\dot{\varepsilon}_2 = \frac{1}{m}\varepsilon_1 - \mu = \frac{1}{m}\varepsilon_1 - \frac{k_1}{r}(x_2 - \bar{x}_2) \tag{19}$$

For system stability, the control law \tilde{u} is chosen as

$$\tilde{u} = -\frac{1}{r}k_d\bar{x}_3 + \mu = -\frac{1}{r}[k_d\bar{x}_3 - k_1(x_2 - \bar{x}_2)] \tag{20}$$

4. SIMULATIONS

The MMC is applied to APVSEA, and the simulation is conducted using ADAMS and Matlab/Simulink. In order to simplify the simulation processing, the APVSEA was built, as shown in figure 13. The car is regarded as a wall if velocity $\tilde{u} = 0$. Therefore, the human force is an external force for this simplified simulation model. In other words, the velocity can move the absolute position of the whole system. But if human force is applied to the block, only the relative position can be changed. The MMC controller was established using Simulink, it receives the datum from ADAMS and feedback velocity command \tilde{u} .

Figure 14 is the APVSEA velocity simulation results, where the blue curve is the reference model's velocity. The simulation input force is $10 \times \sin(3t)$ Newton based on $k_d = 50\text{N/m}$. The green curve represents the APVSEA output velocity under the MMC. From the simulation results, the MMC has a good tracking response. It means the MMC controller can change the plant output response to match to the reference model's response well.

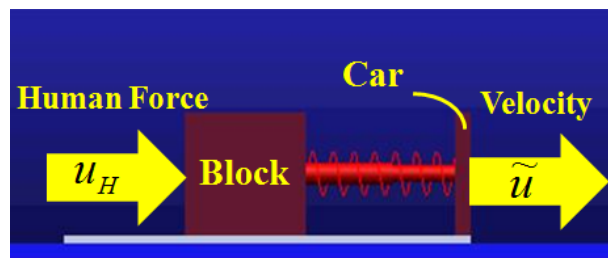


FIGURE 13: The APVSEA Simplify Simulation Model.

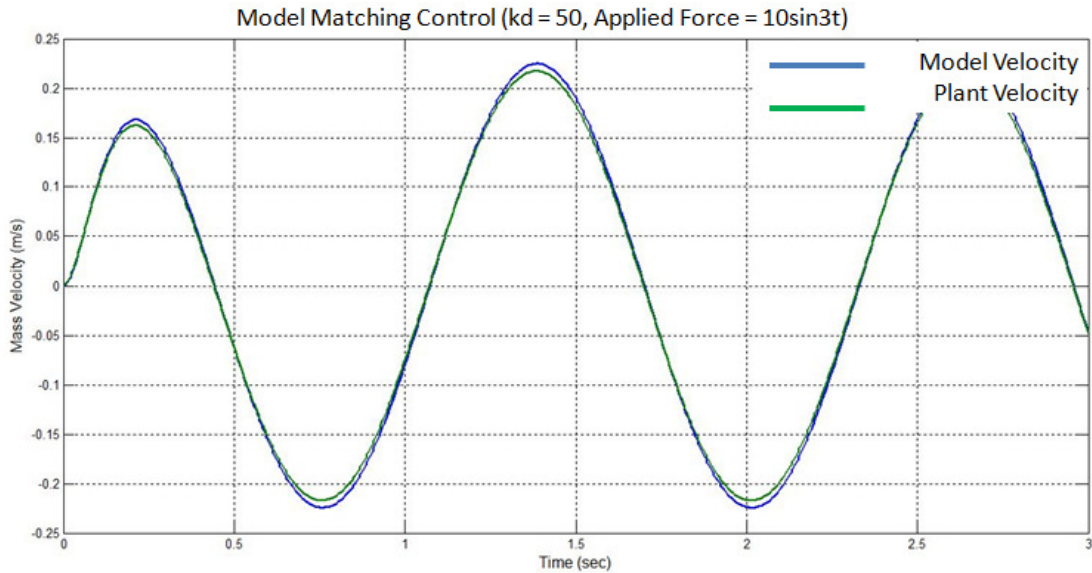


FIGURE 14: The Velocity Response of Mass Block in MMC.

Different stiffness coefficients of spring k_d (140N/m, 50N/m, 0N/m, -50N/m, -140N/m) are tested and analyzed in the simulations, as shown in figure 15. It is worth noting that the simulation with 0N/m stiffness indicates that the response is subject to the condition of the plant without any controller. When the k_d parameter is changed and the same force (3.6N) is applied to the plant, the displacements of the spring under those parameters are different. It means that the stiffness of APVSEA has been changed, and the APVSEA model is matching to the reference model.

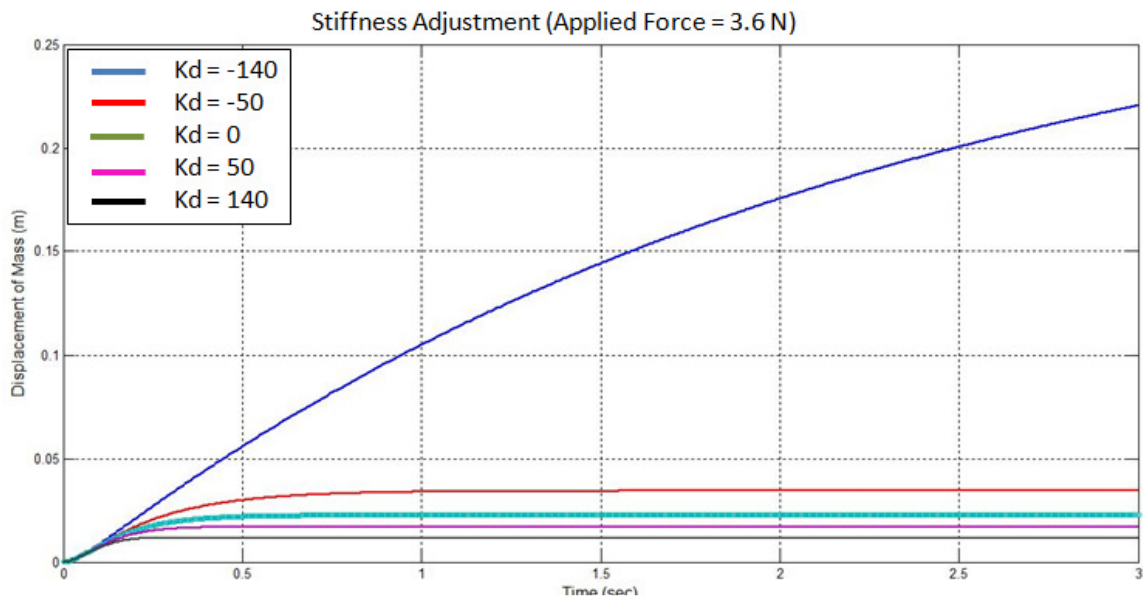


FIGURE 15: The displacement of the spring with different k_d parameters.

The above simulation results show MMC can vary the stiffness of APVSEA well. Since the simulation condition is ideal, the model matching ability still depends on the actuator power or hardware condition in practical case.

5. EXPERIMENTS

Although the APVSEA is an elastic system, it is still insufficient for all applications. However, we can change the APVSEA stiffness using MMC in advance. Through this approach, the user can apply different forces with the same displacement based on different designed stiffness. If the stiffness of the spring is higher, the applied force will be bigger at the same displacement and vice versa.

Figure 16 shows that the stiffness of the APVSEA can be changed by MMC. In the MMC experiments, the user was instructed to apply force to the APVSEA and rotate it to a constant angle. The APVSEA stiffness was changed by MMC, and the user applied forces were simultaneously measured with a potentiometer. In this experiment, the model matching ability which is used to vary the stiffness of APVSEA can be proven. Because the stiffness will affect the displacement of the spring, high/low stiffness generates a smaller/larger displacement.

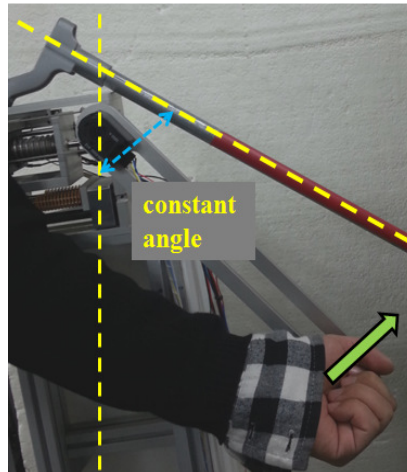


FIGURE 16: Rotate Output Link to Constant Angle.

Figure 17 shows the control structure of the MMC experiment. First, the user applied force to act on the APVSEA system and the feedback displacement of the spring is fed into the MMC. Second, the MMC controller calculates the motor reference and controls the motor to track the reference using proportional-integral-derivative (PID) controller. u_H is the user input force, x_2 is the spring displacement, \tilde{u} is the motor velocity command input, $\dot{\theta}_m$ is the velocity feedback from motor, and τ is the motor torque that drives the APVSEA.

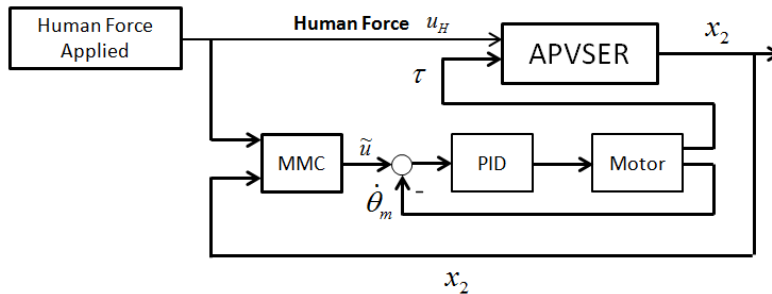


FIGURE 17: The Flow Chart of MMC Experiment.

Figure 18 is the tracking result of the APVSEA output link in the MMC experiment; parameter k_d is -50N/mm . In the result, the green curve shows the model's angle response, i.e., it is a reference input for APVSEA. The red curve represents the APVSEA output link angle in MMC. As shown in the results, MMC had a good angle tracking performance. In other words, APVSEA has

a good model matching ability using MMC, and it can imitate the designed model response very well.

The blue curve represents the force acted on the moving plant and measured by the potentiometer. The actuator of APVSEA is motor 01, and it realizes the MMC control algorithm. The experiment results are shown in Figs. 18 and 19. The user applied force in the same way, but the rotated direction of motor command referred by the MMC controller is different. Since the stiffness parameter k_d is -50N/mm , as in figure 18, this will cause the system's stiffness to decrease and the motor command to be clockwise. However, when the designer sets the stiffness parameter k_d to be 50N/mm , it will cause the whole system's stiffness to increase and the motor command to be counterclockwise (see figure 19).

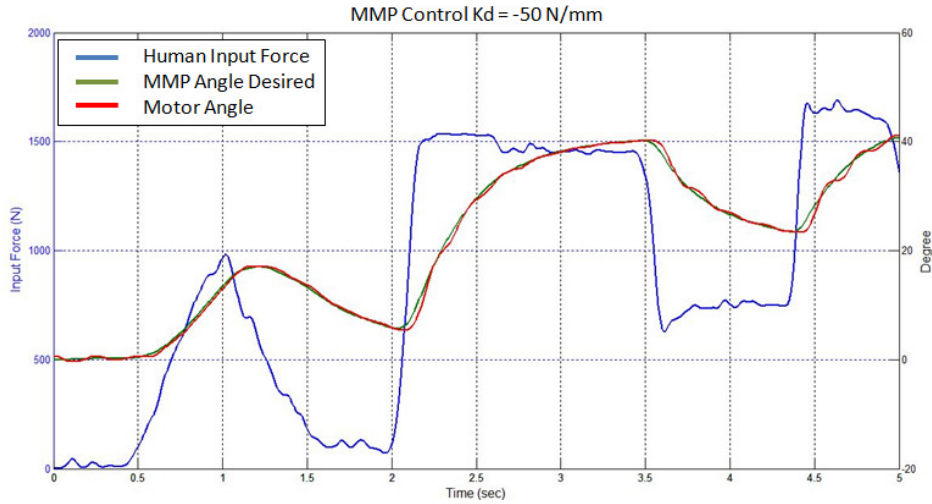


FIGURE 18: k_d is -50N/mm .

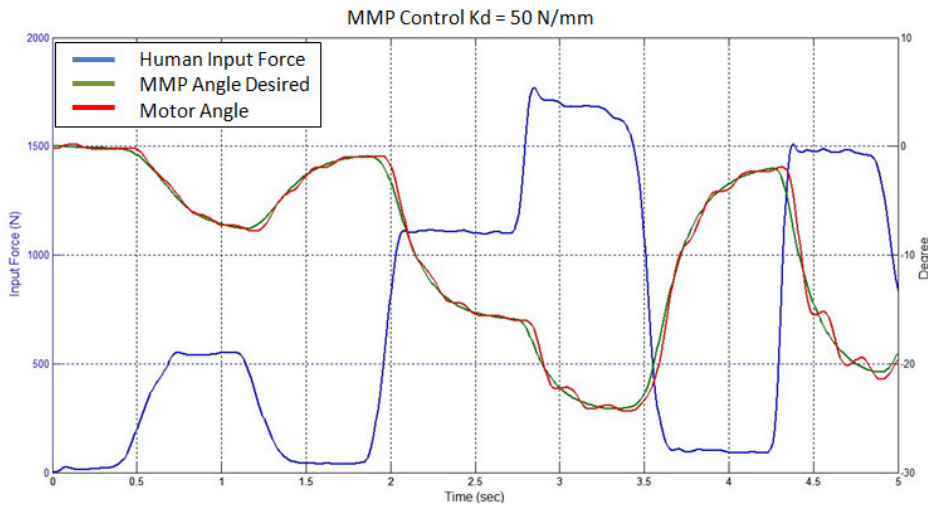


FIGURE 19: k_d is 50N/mm .

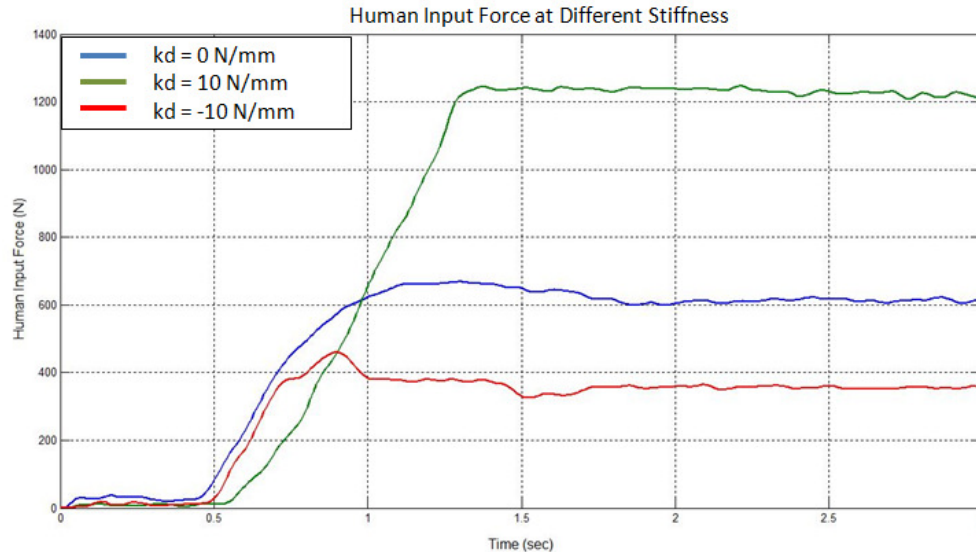


FIGURE 20: The user applied different forces at different designed system's stiffness.

As mentioned above, the user applies force to the same position depending on the system's stiffness—the higher the stiffness the bigger the force. Figure 20 shows the user applied force to the output link. The blue curve, where parameter k_d is zero, shows that the APVSEA is unaffected by the MMC controller. In other words, this is the intrinsic response of the APVSEA. When $k_d = 0$ N/mm, it needs approximately 600N when the user rotated the output link to a constant angle. The stiffness which is shown by the green curve is 162N/mm because the parameter spring is set to $k_d = 10$ N/mm. For the case of the green curve, the user needs to apply nearly 1200 N to the output link. However, if the parameter is set to $k_d = -10$ N/mm, the system's stiffness will decrease. The user only needs to provide a force of 380N to rotate the output link to a constant angle.

6. CONCLUSION

With the more widespread applications of robots, the SEA with a constant stiffness cannot satisfy various applications in the future. There is a need to consider the safety ability with human-robot interaction applications. Nevertheless, if the system varies the stiffness using mechanical approach, it will increase the system's volume and weight. Therefore, this paper proposes a non-back drivable APVSEA system with MMC. The bond graph method can be used to integrate motors and electrical circuits and can easily extend the model to a robotic arm, exoskeleton system design, or human-robot interaction model. In order to change the system's stiffness actively, we designed the MMC to vary APVSEA's stiffness. MMC can control the plant in order to track the model's performance. This paper offers complete MMC controller design steps using bond graph by checking solvability, finding an inverse system, solving DDP, deriving error dynamics, and performing an asymptotic analysis.

From the simulation and experiment results, the MMC controller can change the APVSEA stiffness very well. The proposed MMC variable stiffness APVSEA system can be safely applied to human-robot interaction.

7. FUTURE WORK

Model Matching Control had been developed using bond graph approach. It can be used to change system's stiffness. However, this approach can be applied to human robot safe interaction. Decreasing or stopping robot's working velocity is a common method for guaranteeing human safe in the factory, but it will cause the robot has low working efficiency. Therefore, we can modify robot's stiffness without decreasing or stopping its working velocity for keeping human safe. The benefit of this future work is human can co-work with robot in safety environment.

8. REFERENCES

- [1] R.J. Wang, H.P. Huang, "An Active-Passive Variable Stiffness Elastic Actuator for Safety Robot Systems", IEEE/RSJ International Conference on Intelligent Robots and Systems (IROS), Taipei, pp. 3664-3669, Oct. 18-22, 2010.
- [2] K. Kong, J. Bae, M. Tomizuka, "A Compact Rotary Series Elastic Actuator for Human Assistive Systems," IEEE/ASME Transactions on Mechatronics, Vol. 17, No. 2, pp. 288 - 297, April 2012.
- [3] M. Grun, R. Muller, U. Konigorski, "Model based control of series elastic actuators," International Conference on Biomedical Robotics and Biomechatronics (BioRob), Roma, pp. 538 – 54, June 2012.
- [4] K. Kong, J. Bae, M. Tomizuka, "Control of Rotary Series Elastic Actuator for Ideal Force-Mode Actuation in Human-Robot Interaction Applications," IEEE/ASME Transactions on Mechatronics, Vol. 14, No. 1, pp. 105-118, 2009.
- [5] J. W. Sensinger, R. F. Weir, "Design and Analysis of a Non-backdrivable Series Elastic Actuator," IEEE International Conference on Rehabilitation Robotics, Chicago, IL, USA, pp. 390-393, June 2005.
- [6] E. Torres-Jara, and J. Banks, "A Simple and Scalable Force Actuator," 35th International Symposium on Robotics, 2004.
- [7] G. Wyeth, "Demonstrating the Safety and Performance of a Velocity Sourced Series Elastic Actuator," IEEE International Conference on Robotics and Automation, Pasadena, CA, USA, pp. 3642–3647, May 2008.
- [8] J. Choi, S. Hong, W. Lee and S. Kang, "A Variable Stiffness Joint using Leaf Springs for Robot Manipulators," IEEE International Conference on Robotics and Automation Kobe Internal Conference Center, Kobe, Japan, pp. 4363-4368, May 2009.
- [9] R.J. Wang, and H.P. Huang, "Active Variable Stiffness Elastic Actuator: Design and Application for Safe Physical Human-Robot Interaction," IEEE International Conference on Robotics and Biomimetics (ROBIO), Tianjin, China, pp. 1417-1422., December 2010.
- [10] J.J. Park, Y.J. Lee, J.B. Song and H.S. Kim, "Safe Joint Mechanism based on Nonlinear Stiffness for Safe Human-Robot Collision," International Conference on Robotics and Automation, Pasadena, CA, USA, pp. 2177–2182, May 2008.
- [11] H.S. Kim, J.J. Park and J.B. Song, "Safe Joint Mechanism using Double Slider Mechanism and Spring for Humanoid Robot Arm," IEEE International Conference on Human Robots, Daejeon, Korea, pp. 73–78, December 1~3, 2008.
- [12] J.J. Park, B.S. Kim, J.B. Song and H.S. Kim, "Safe Link Mechanism based on Passive Compliance for Safe Human Robot Collision," IEEE International Conference on Robotics and Automation, Roma, Italy, pp. 1152–1157, April 2007.
- [13] J.J. Park, H.S. Kim and J.B. Song, "Safe Robot Arm with Safe Joint Mechanism using Nonlinear Spring System for Collision Safety," IEEE International Conference on Robotics and Automation, Kobe, Japan, pp. 3371–3376, May 2009.
- [14] S.A. Migliore, E.A. Brown, and S.P. DeWeerth, "Biologically Inspired Joint Stiffness Control," IEEE International Conference on Robotics and Automation, Barcelona, Spain, pp. 4508–4513, April 2005.

- [15] S. Wolf and G. Hirzinger, "A New Variable Stiffness Design: Matching Requirements of the Next Robot Generation," IEEE International Conference on Robotics and Automation, Pasadena, CA, USA, pp. 1741–1746, May 2008.
- [16] R. Ghorbani, and Q. Wu, "Closed Loop Control of an Intentionally Adjustable Compliant Actuator," American Control Conference, Minneapolis, Minnesota, USA, pp. 3235–3240, June 2006.
- [17] N. Saga, T. Saikawa and H. Okano, "Flexor Mechanism of Robot Arm using Pneumatic Muscle Actuators," IEEE International Conference on Mechatronics & Automation, Niagara Falls, Canada, Vol. 3, pp. 1261–1266, July 2005.
- [18] R. Hernani, G. Romero, and M.L. Martinez, "A Musculoskeletal Human Gait Model using the Bond Graph Technique," World Congress of Biomechanics (WCB 2010), Singapore, Vol. 31, pp 270-273, August 2010.
- [19] G. Golo, van der Schaft, Arjan, P.C. Breedveld, B.M. Maschke., "Hamiltonian Formulation of Bond Graphs," Nonlinear and Hybrid Systems in Automotive Control, London, pp. 351-372, 2003.
- [20] D. Vink, D.J. Balance, P. Gawthrop, "Bond graphs in Model Matching Control," Mathematical and Computer Modelling of Dynamical Systems, Vol. 12, No. 2, pp. 249-261, 2006.
- [21] D. Vink, "Aspects of Bond Graph Modelling in Control," Doctoral Dissertation, Department of Mechanical Engineering, Glasgow University, 2005.
- [22] R.F. Ngwompo, S. Scavarda, and D. Thomasset, "Physical Model-Based Inversion in Control Systems Design using Bond Graph Representation Part 1: Theory," Institution of Mechanical Engineers, Part I: Journal of Systems and Control Engineering, Vol. 215, No. 2, pp. 95-104, 2001.
- [23] M. Wlasowski, and F. Lorenz, "How to Determine the Solvability of Bond Graph Linear Junction Structures," Journal of the Franklin Institute, Vol. 328, No. 5, pp. 855-869, 1991.